CHAPTER 9

Magnetic Actuator Transient Operation

While the preceding two chapters analyzed magnetic actuators under DC and AC operation, they did not consider the transient effects of turning on (or off) the DC and AC currents or voltages. This chapter is the first to investigate transient operation of actuators. Its techniques will help determine actuator performance for any applied voltage or current versus time.

9.1 BASIC TIMELINE

The basic timeline for transient operation of magnetic actuators is the following.

(1) An energizing circuit turns on, supplying voltage and current.
(2) The coil current rises, partly determined by an electrical time constant.
(3) The magnetic flux density rises, partly determined by a time constant called the magnetic diffusion time or nonlinear infusion time.
(4) The force rises as the magnetic flux density rises.
(5) The force produces acceleration of the armature and/or attached mass.
(6) After a certain time, during which the armature may or may not reach the end of its stroke, the energizing circuit may be turned off. If the current suddenly becomes zero, then the magnetic flux density (and related force) falls, partly determined by the magnetic diffusion time or nonlinear effusion time.

Each of the above steps may introduce a time delay. For many applications, a time delay is undesirable because it slows the speed of response.

This chapter studies the basics of steps 3, 4, 5, and 6 above. Steps 1 and 2 will not be investigated until Chapters 12, 14, and 15, which will examine further aspects of transient operation.

Magnetic Actuators and Sensors, Second Edition. John R. Brauer.
© 2014 The Institute of Electrical and Electronics Engineers, Inc. Published 2014 by John Wiley & Sons, Inc.

9.2 SIZE, FORCE, AND ACCELERATION

Magnetic force is the most important parameter of magnetic actuators, and it determines the mechanical acceleration and speed of response of the actuator. While many aspects of the mechanical performance will not be studied until Chapters 14–16, here some basic relations between force and actuator size are presented.

The force for axisymmetric plunger actuators of the type shown in Figure E7.4.1 is related to the actuator of a more general design shown in Figure 9.1. Both designs have the plunger and its stopper extending to the same radius, but in Figure 9.1 their inner radius may be greater than zero. Thus the cylindrical plunger of radius R_p may be hollow, with its end having area $k_a \pi \ R_p^2$ instead of $\pi \ R_p^2$, where k_a is an area constant less than or equal to one.

For a cylindrical plunger of length L_p, the optimum design would have the same area for magnetic flux entering through the side and leaving the circular end of the plunger:

$$2\pi R_p L_p = k_a \pi R_p^2 \tag{9.1}$$

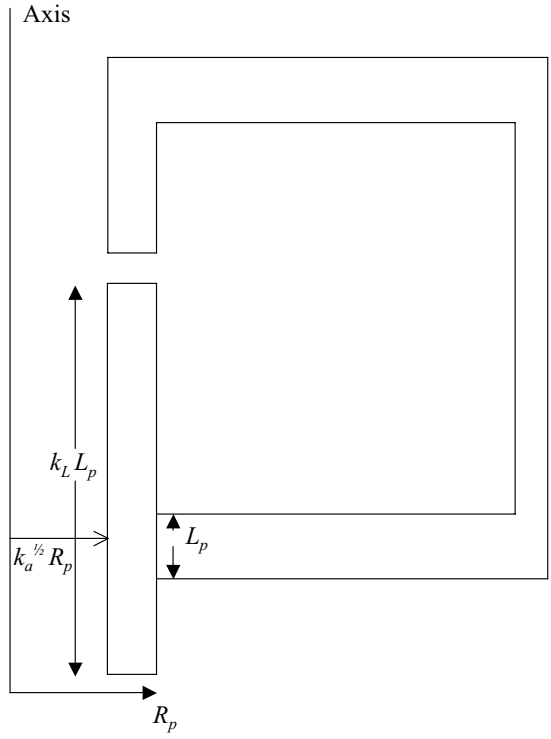

FIGURE 9.1 Dimensional parameters of axisymmetric plunger actuator.

Hence:

$$L_p = k_a R_p/2 \tag{9.2}$$

would be the minimum plunger length. However, in many cases, such as in the actuator of Figure 9.1, the actual plunger length is longer. Denoting the actual length as $k_L L_p$, where k_L is a constant greater than or equal to one, the plunger volume is:

$$v = k_L L_p \left(k_a \pi\ R_p^2\right) = k_L \left(\pi k_a^2\ R_p^3\right)/2 \tag{9.3}$$

The acceleration is:

$$a = F/m = P\left(\pi k_a R_p^2\right)/(\rho\, v) \tag{9.4}$$

where P is the magnetic pressure and ρ is the mass density of the plunger material. It has been shown in Chapter 5 that for typical steel the maximum magnetic pressure $P = 20.\text{E5N/m}^2$. Therefore the maximum acceleration of the cylindrical plunger is:

$$a = 20.\text{E5}\left(\pi\ k_a\ R_p^2\right) / \left(\rho\left(\pi\ k_L k_a^2\ R_p^3\right)/2\right) \tag{9.5}$$

$$a = 40.\text{E5}/(\rho\, k_L k_a\ R_p) \tag{9.6}$$

For steel $\rho = 7800\ \text{kg/m}^3$, and thus:

$$a = 513/(R_p k_L k_a) \tag{9.7}$$

Thus to maximize acceleration, $k_L k_a R_p$ should be minimized; that is, the smaller the plunger, the faster it will move, assuming there are no other forces than the magnetic force. This speedier acceleration of small objects is commonly observed in nature; for example, a 2-g hummingbird accelerates much faster than a 10-kg turkey.

If the actuator of Figure 9.1 is the Bessho actuator of Figure 5.2, then the above dimensions are known. With $R_p = 20\text{E}{-3}$ m, the area constant $k_a = 1$, and the length constant $k_L = 2\pi(0.02)(0.142)/\pi(0.02)^2 = 14.2$. Then (9.7) gives $a = 1806\ \text{m/s}^2$. If this acceleration exists over the entire stroke s, then:

$$s = {}^1\!/_2\, at^2 \tag{9.8}$$

or

$$t = (2s/a)^{0.5} \tag{9.9}$$

For example, if $s = 10\text{E}{-3}$ m, (9.9) gives $t = 3.33$ ms. Note that this is the *minimum possible stroke time* for the Bessho actuator with no opposing forces or masses on the armature. Actual stroke times either experimentally observed [1] or computed using time-stepping finite-element analysis [2] are 51 ms or greater.

For other types of actuators, such as the clapper types of Chapter 7, similar simple equations can be developed. Thus the maximum force and minimum operation times can be estimated.

The above minimum stroke time assumes that the magnetic pressure is always the maximum. Thus it requires high current, which usually requires a significant rise time, and zero time for the magnetic field to diffuse through the plunger. The actual time for the magnetic field to diffuse is the subject of the next sections. Throughout this chapter, unless otherwise indicated, the hysteresis loop of the steel is assumed to be negligibly small.

9.3 LINEAR MAGNETIC DIFFUSION TIMES

Magnetic diffusion time τ_m is a useful parameter for predicting eddy current delay effects on transient magnetic fields and related parameters such as inductance and force. This section examines diffusion times in conducting materials with linear *B–H* curves, that is, with constant magnetic permeability μ.

9.3.1 Steel Slab Turnon and Turnoff

The *diffusion equation* is derived starting with Maxwell's equations which obtained (8.21) in Chapter 8:

$$\nabla \times \sigma^{-1} \nabla \times \mathbf{H} = -\frac{\partial \mathbf{B}}{\partial t} \tag{9.10}$$

which for constant uniform conductivity σ and permeability μ becomes:

$$\frac{1}{\mu\sigma} \nabla \times \nabla \times \mathbf{B} = -\frac{\partial \mathbf{B}}{\partial t} \tag{9.11}$$

Using vector identities we obtain the *vector diffusion equation* [3]:

$$\frac{1}{\mu\sigma} \nabla^2 \mathbf{B} = \frac{\partial \mathbf{B}}{\partial t} \tag{9.12}$$

Figure 9.2 shows a *C*-core similar to that of Figure E3.1.1 except that its gap is now filled with a conducting slab. As in Example 8.1, the conducting material is assumed to extend in the $+z$ and $-z$ directions out of the page to obtain zero end region resistance for its eddy currents which elsewhere flow only in the $+z$ and $-z$ directions. As in Figure E3.1.1, throughout the entire 2D problem region the fields are assumed to be independent of z. The slab is assumed to have **B** that only varies in the

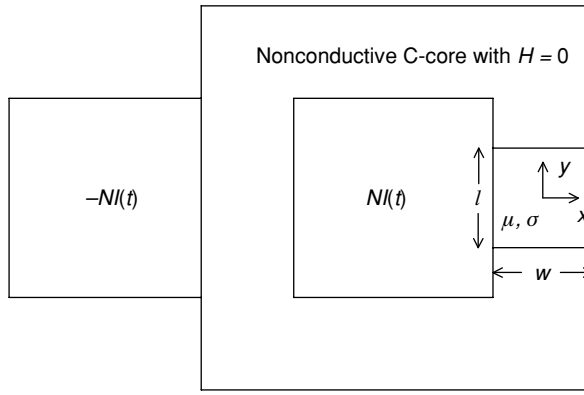

FIGURE 9.2 Conducting slab filling the gap of a planar *C*-core made of nonconducting high permeability ($H = 0$) material. The fields and eddy currents in the slab are assumed to vary only in the x direction, and the eddy currents are assumed z-directed except at the slab ends which have zero voltage drops. The current $I(t)$ is first assumed to be turned on at time zero.

x direction and only has a y component. Thus in the conducting region of Figure 9.2, (9.12) becomes the *1D slab diffusion differential equation* [3]:

$$\frac{1}{\mu\sigma}\frac{\partial^2 B_y}{\partial x^2} = \frac{\partial B_y}{\partial t} \tag{9.13}$$

The current $I(t)$ in Figure 9.2 is initially assumed to be zero before time zero and to be turned on as a step (with zero rise time) at time zero. In this "turnon" case, B throughout the slab must be zero at time zero, and then must gradually increase. After a sufficiently long time all transient eddy currents in the slab will die out and B_y will be uniform in the slab with its final (DC) value B_F obeying Ampere's law. With these boundary conditions for the diffusion equation (9.13), its solution is:

$$B_y = B_F\left[1 - \sum_{n=\text{odd}}\left(\left(\frac{4}{n\pi}\right)\sin\left(n\pi\left(\frac{1}{2} - \frac{x}{w}\right)\right)e^{-n^2 t/\tau_m}\right)\right] \tag{9.14}$$

where the *diffusion time* is:

$$\tau_m = \mu\,\sigma(w/\pi)^2 \tag{9.15}$$

where w is the width of the conducting slab as shown in Figure 9.2. When the step rise in current and $H(t)$ is applied, the magnetic flux density B diffuses inward (infuses) from both slab sides (coil regions), for example, moving in the x direction from its left side to the right and from its right side to the left, as shown in Figure 9.3. The fundamental Fourier component of the flux reaches 63% of its final value in the middle of the conducting slab at $t = \tau_m$. Figure 9.3 plots the magnetic flux density

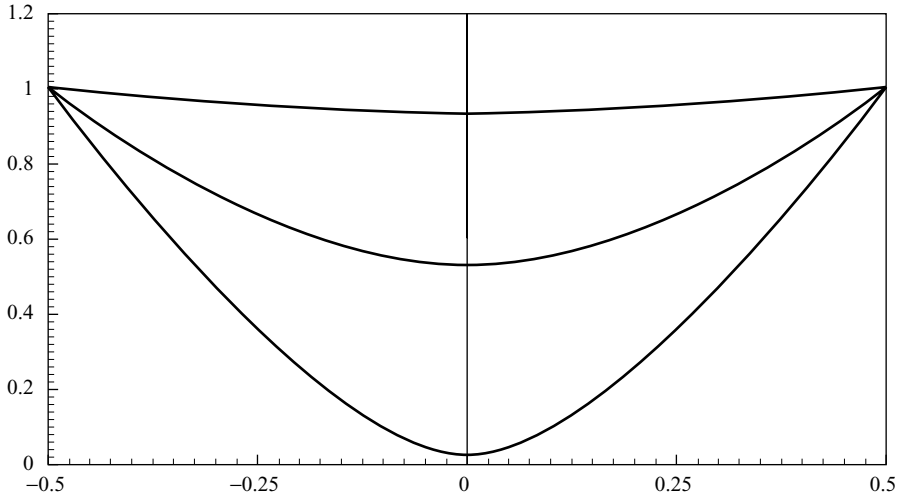

FIGURE 9.3 Computer display of analytical results using (9.14) for diffusion into a steel slab with constant permeability. The top curve is for $t = 3\ \tau_m$, the middle curve is for $t = \tau_m$, and the lower curve is for $t = 0.3\ \tau_m$. The vertical axis is $B(t)/B_F$, and the horizontal axis is x/w.

versus the position of (9.14) at various times, showing the inward diffusion. Note that the *total* flux density in the middle of the conducting slab at $t = \tau_m$ reaches 53.2% of the final value, a change from the exponential 63% due to only the fundamental component.

If the DC coil current has existed over many diffusion times and is suddenly switched off, the current and $H(t)$ then undergo a step decrement. The magnetic flux density B diffuses outward (effuses) to both slab sides, decaying most slowly in the center of the slab. Thus the magnetic force will also eventually decay to zero. However, if the steel is a hard magnetic material as discussed in Chapter 5, then it will have significant coercive field intensity H_c and residual flux density B_r, and there may be a significant permanent magnet force. For soft steels, however, the permanent magnet force is usually less than 1% of the steady-state force when energized. For a current step decrement at time zero, the flux density of (9.14) becomes:

$$B_y = B_o \sum_{n=\text{odd}} \left[\left(\frac{4}{n\pi} \right) \sin \left(n\pi \left(\frac{1}{2} - \frac{x}{w} \right) \right) e^{-\frac{n^2 t}{\tau_m}} \right] \tag{9.16}$$

where B_o is the initial flux density (in the y direction). At time $t = \tau_m$ the maximum flux density B_y in (9.16) is 47% of B_o and is located at $x = 0$, in the middle of the slab.

Magnetic infusion and effusion in a steel slab can be likened to a dry rectangular sponge that is immersed in a pail of water. The water will infuse inward from the outer sponge walls until the entire sponge is wet. Then if the sponge is set out in

air, its water will effuse outward with the outer walls drying first and the inside drying last.

Example 9.1 Magnetic Diffusion into Linear Steel Slab During Turnon and Turnoff Figure E9.1.1 shows a large planar magnetic device made up of one coil, solid steel, and laminated steel. All steel is of depth 1 m. There is no airgap between the solid armature and the laminated stator. The laminations have relative permeability of 100,000 and zero conductivity. Figure E9.1.2 shows a 1D slice through the right half of Figure E9.1.1 with width $w = 0.447$ m. The slice is used because diffusion time of (9.15) is a 1D concept. The conductivity of the armature is assumed to be 1.7E6 S/m, and its B–H curve is assumed to obey an equation for cast steel of Chapter 2:

$$H = (49.4e^{1.46B^2} + 520.6)B \tag{E9.1.1}$$

which for low B–H has a relative permeability of 1344.

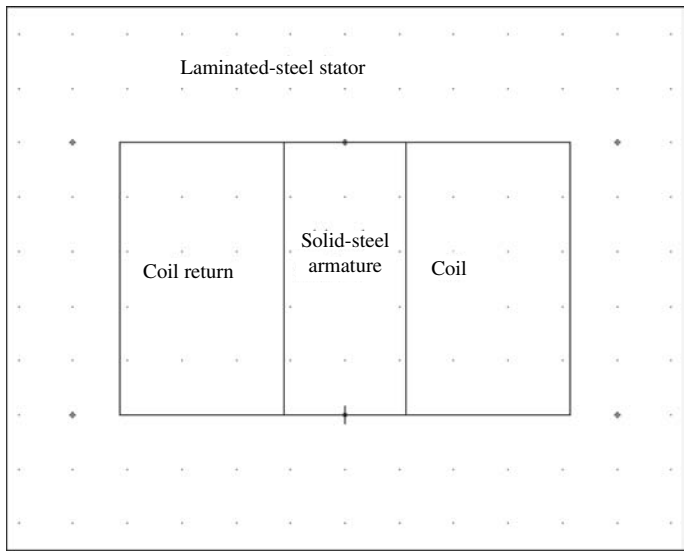

FIGURE E9.1.1 Computer display of large magnetic device. Its depth is 1 m. The solid armature is of (x,y) dimensions 0.447 by 1.0 m. Both coil regions are of dimension 0.6055 by 1.0 m. The laminated stator has overall dimensions 2.49 by 2.0 m.

FIGURE E9.1.2 Computer display of slice of Figure E9.1.1 for use in determining diffusion. The rotor core has half width equal to the dimension $T1 = 0.2235$ m in Figure E9.1.1. The armature has conductivity 1.7E6 S/m and relative permeability of 1344. The stator has zero conductivity and relative permeability of 100,000. The computed magnetic flux lines are shown at $t = 100$ s after the winding current decrement.

Assuming $NI = 264$ ampere-turns has existed for a long time in Figure E9.1.1, and is switched off at time zero, the following are to be found.

(a) Use (9.15) to calculate the diffusion time.
(b) Use Maxwell's magnetostatic solver to obtain the flux line plot and energy at time zero for the entire device and for the slice.
(c) Use the 2D planar transient finite-element solver of Maxwell (not included in the student version SV) to find the flux line plot at $t = 100$ s, and also graph B versus x at $t = \tau_m$, and compare it with (9.16).

Solution

(a) The diffusion time τ_m for Figure E9.1.2 is found using (9.15) with $w = 0.447$ m to be 58.14 s.
(b) For the entire device, Maxwell obtains an energy of 25.74 J. For the slice, which has only 5% of the ampere-turns, the ampere-turns are reduced to 13.2, and the energy computed by Maxwell is reduced to 0.65 J, which is approximately 2.5% of the energy of the entire device, as it should be. In both models, the flux density in the armature is approximately 0.4427 T.
(c) The "Transient" Solver in Maxwell 2D was used to obtain the flux density distribution computed in Figure E9.1.2 at $t = 100$ s. Note that the laminated stator has uniform flux density but the solid armature has a nonuniform flux density with lowest value on its surface.

The computed flux density at 58 s for the finite-element model of Figure E9.1.1 is graphed by the postprocessor in Figure E9.1.3. The center value of 0.2073 T is 47% of the initial $B_o = 0.4427$ T throughout the armature, and thus the computed

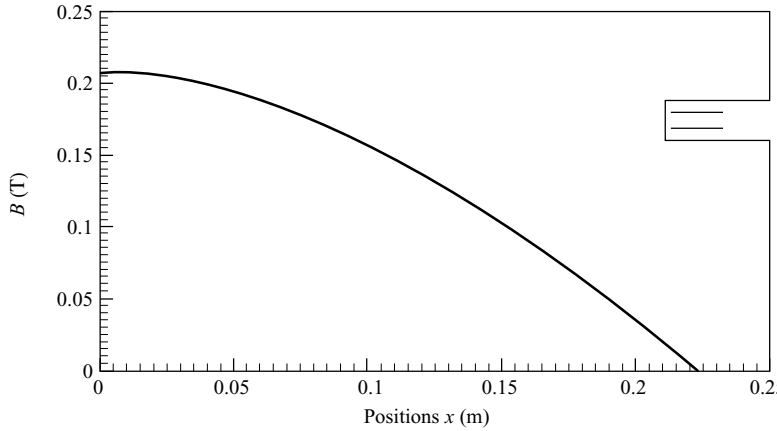

FIGURE E9.1.3 Graph of B versus x for model of Figure E9.1.2 at time $t = 58$ s, which is close to the computed diffusion time using (9.16). Note that the dark theoretical curve of (9.12) lies on top of the lighter curve computed by transient finite-element analysis.

diffusion time agrees closely with the 58.14 s predicted by (9.15). In Figure E9.1.3 the curve of finite-element results lies on top of the analytical curve from (9.16).

9.3.2 Steel Cylinder

Because many actuators, including the Bessho actuator of Figure 5.2, have cylindrical plunger armatures and cylindrical stoppers made of solid steel, magnetic diffusion in cylinders is important. The eddy current induced in axisymmetric objects such as cylinders circles around the z axis of symmetry and thus there are no end effects (unlike in the previous planar slab). The vector magnetic diffusion equation (9.12) for cylindrical coordinates of radius r and axial position z becomes the *1D cylindrical diffusion differential equation*:

$$\frac{1}{\mu\sigma}\frac{1}{r}\frac{\partial}{\partial r}\left(r\frac{\partial B_z}{\partial r}\right) = \frac{\partial B_z}{\partial t} \tag{9.17}$$

where the factors $(1/r)$ and r come from the expression for curl in cylindrical coordinates. The solution for this differential equation for boundary conditions (as for the previous slab case) of zero flux density until time zero, when a step increment in current is applied, is the equation [3]:

$$B_z = B_F\left[1 - \sum_{i=1,2,3} C_i J_o\left(\upsilon_i \frac{r}{R}\right) e^{-t/\tau_{mi}}\right] \tag{9.18}$$

where B_F is the final flux density long after the step current is turned on, R is the outer radius of the cylinder, and J_o is the Bessel function of the first order with the first three roots $\upsilon_1 = 2.4048$, $\upsilon_2 = 5.5201$, and $\upsilon_3 = 8.6537$. The constant coefficients in (9.18) can be shown to be $C_1 = 1.602$, $C_2 = -1.066$, $C_3 = 0.851$, followed by less important ones. Using (9.18), at time $t = \tau_m$ the flux density along the cylinder axis has the fundamental component of 63% of the final value B_F, but the *total* flux density at that time along the axis is only 41.62% of B_F. In (9.18) τ_{mi} is the same as τ_m for $i = 1$, and in general obeys:

$$\tau_{mi} = \mu\,\sigma(R/\upsilon_i)^2 \tag{9.19}$$

Thus the diffusion time τ_m for a cylinder with constant permeability is defined using the first root to give [3]:

$$\tau_m = \mu\sigma\ R^2/(2.4048)^2 \tag{9.20}$$

For the Bessho actuator of Figure 5.2, the conductivity of all steels is specified as 1.7E6 S/m [1]. There are two different B–H curves specified. One is for the armature and stopper of Figure 5.2 and the other is for the yoke. The cylindrical armature B–H curve is given in Table B2.2 and Figure B2 of Appendix B; it begins with a constant permeability of 630 times that of air. The resulting magnetic diffusion time τ_m using

(9.20) is 93 ms. However, nonlinear finite-element computations [2] have obtained closing times for the Bessho actuator with the above steel as low as 51 ms, so the diffusion time τ_m of (9.20) appears to be longer than actual nonlinear diffusion time.

If the DC coil current has existed over many diffusion times and is suddenly switched off, the current and $H(t)$ then undergo a step decrement. The magnetic flux density B diffuses outward toward the surface of the cylinder, so instead of (9.18) the flux density for $H(t)$ turned off at $t = 0$ is:

$$B_z = B_o \left[\sum_{i=1,2,3} C_i J_o \left(\upsilon_i \frac{r}{R} \right) e^{-t/\tau_{mi}} \right] \tag{9.21}$$

where B_o is the initial flux density (in the z direction). At time $t = \tau_m$ the maximum flux density B_z in (9.21) is 58.38% of B_o and is located at zero radius. Magnetic infusion and effusion in a steel cylinder can be likened to a dry roll of paper towels (with zero interior radius) that is immersed in water. The water will infuse inward from the outer radius until the entire roll is wet. Then if the roll is set out in air, its water will effuse outward with the outer radius drying first and the inside drying last.

9.4 NONLINEAR MAGNETIC INFUSION TIMES

The formulas for magnetic diffusion time τ_m in all the preceding section contain permeability μ. Many magnetic devices contain steel operated in the nonlinear region of its B–H curve, and thus the value of μ cannot be determined. The effect of a nonlinear B–H curve on diffusion time must be investigated. It will be found that the nonlinear diffusion time not only depends on the magnitude of the applied H, but also depends on whether the applied H is being turned on or being turned off. When current and H are turned on, the magnetic field B diffuses inward with a diffusion time called *infusion* time. This section examines infusion times, while the next section will examine *effusion* times which apply when current and H are turned off and the magnetic field B leaves or effuses from the conducting material.

9.4.1 Simple Equation for Steel Slab with "Step" *B–H*

To obtain an approximate formula for τ_m in nonlinear planar slabs, first assume a "step" B–H curve [4] with infinite slope from $B = 0$ to B_m and zero slope for $B > B_m$. This simple B–H curve has been shown to respond to an applied field intensity $H_o(t)$ by producing a traveling flux density wavefront of position $x_o(t)$ given by [4]:

$$x_o(t) = \left[\int H_o(t) dt / (1/2 \, \sigma B_m) \right]^{1/2} \tag{9.22}$$

where $1/2$ is placed in the denominator because the applied $H_o(t)$ here starts at zero, not $-B_m$ as assumed in [4]. Assuming a planar slab of width w with $H_o(t)$ stepped to H_o on both slab sides ($x = 0$ and $x = w$), then $x_o(t) = w/2$ at time $t = \tau_m$. Then the

integral is replaced by $H_o \tau_m$, resulting in the formula for nonlinear planar magnetic diffusion time with step *B–H*:

$$\tau_m = \sigma w^2 B_m / (8 H_o) \tag{9.23}$$

9.4.2 Transient Finite-Element Computations for Steel Slabs

The infusion time τ_m for devices with nonlinear *B–H* curves may be computed using transient finite-element analysis of the type used in Example 9.1. Various *B–H* curves may be input, both the preceding "step" curve and curves of actual steels.

Example 9.2 Magnetic Infusion in Nonlinear Rectangular Inductor The first example of applying (9.23) is to the rectangular inductor shown in Figure E9.2.1. The entire rectangular core of this inductor is 45 mm wide and 90 mm high and assumed made of solid steel. The magnetic field and eddy currents are assumed to be invariant

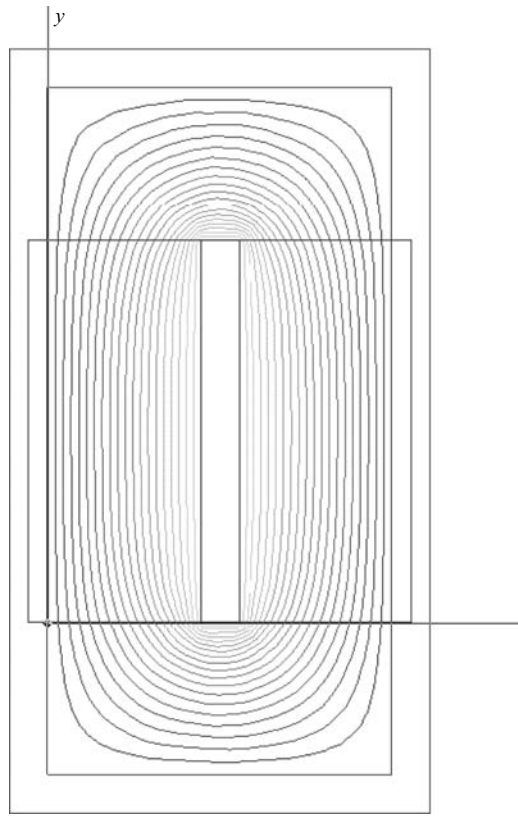

FIGURE E9.2.1 Rectangular planar inductor, showing typical magnetostatic flux lines computed by 2D planar finite-element analysis. The solid steel is a hollow rectangle consisting of four legs of width 20 mm, with copper windings on its left and right legs carrying currents that produce magnetic flux as shown. The window in the center of the legs is of size 5 by 50 mm.

with dimension z (out of the page), and thus the fields vary only in the xy plane. To achieve such independence of z, the depth of the inductor into the page must be much greater than its dimensions in the xy plane. The eddy currents in the steel core of conductivity 1.7E6 S/m flow in the $\pm z$ direction and must sum to zero according to Kirchhoff's current law. Each of the two coils in Figure E9.2.1 has 660 turns.

Then

(a) The nonlinear infusion time is to be found using (9.23) assuming a step curve at $B_m = 2$ T for coil currents of 0.5, 1, and 2 A. Also, find its magnetostatic flux lines using Maxwell and constant steel relative permeability of 2000.

(b) Using Maxwell 2D or other available nonlinear transient finite-element software, confirm the results of (9.23) and then use the actual armature steel B–H curve given in [1]. To save computer time, a slice model can be used as in Example 9.1.

Solution

(a) The infusion time τ_m for Figure E9.2.1 is found using (9.23) as follows. The width $w = 0.020$ m in Figure E9.2.1. The applied field intensity H_o is found using Ampere's law:

$$(H_o)(2 \times 0.050) = 2(660)I \tag{E9.2.1}$$

$$H_o = 13{,}200\, I \tag{E9.2.2}$$

The resulting three τ_m values are listed in Table E9.2.1. Note that all three values are much less than the 54.6 ms obtained by the linear formula (9.15), and that the higher the current, the smaller the infusion time. The computed flux lines are shown in Figure E9.2.1.

(b) Rather than model the entire planar region of Figure E9.2.1, because the inductor dimension in the y direction is considerably greater than that in the x direction, the slice model of Figure E9.2.2 can be used. Its dimension in the y direction is only 2 mm. Because eddy currents and skin effects must be modeled, a fairly fine finite-element mesh is required, and thus the reduced computer time obtained by the reduced model of Figure E9.2.2 is helpful.

TABLE E9.2.1 Nonlinear Magnetic Infusion Times for Figure E9.2.2 (ms)

I (A)	H_o (A/m)	Analytical (9.17)	FEA (Step B–H)	FEA (Real B–H)
0.5	6600	25.8	25.0	18.9
1.0	13,200	12.9	12.5	9.0
2.0	26,400	6.4	6.2	5.0

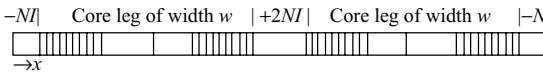

FIGURE E9.2.2 Two millimeter high section of Figure E9.2.1. Computed flux lines are for $t = 4$ ms and real B–H curve. Note that the flux lines are diffusing inward from the four outer steel core surfaces with windings of conductors N containing current $I = 1$ A.

The windings in Figure E9.2.2 contain a step current $I(t)$ and number of conductors N. The N in Figure E9.2.2 must be (2 mm)/(50 mm) times the 660 turns of Figure E9.2.1, and thus $N = 26.4$.

Transient finite-element analysis was first used to obtain the infusion time for low H_o values, for which the relative steel permeability is 630. Ansoft's Maxwell

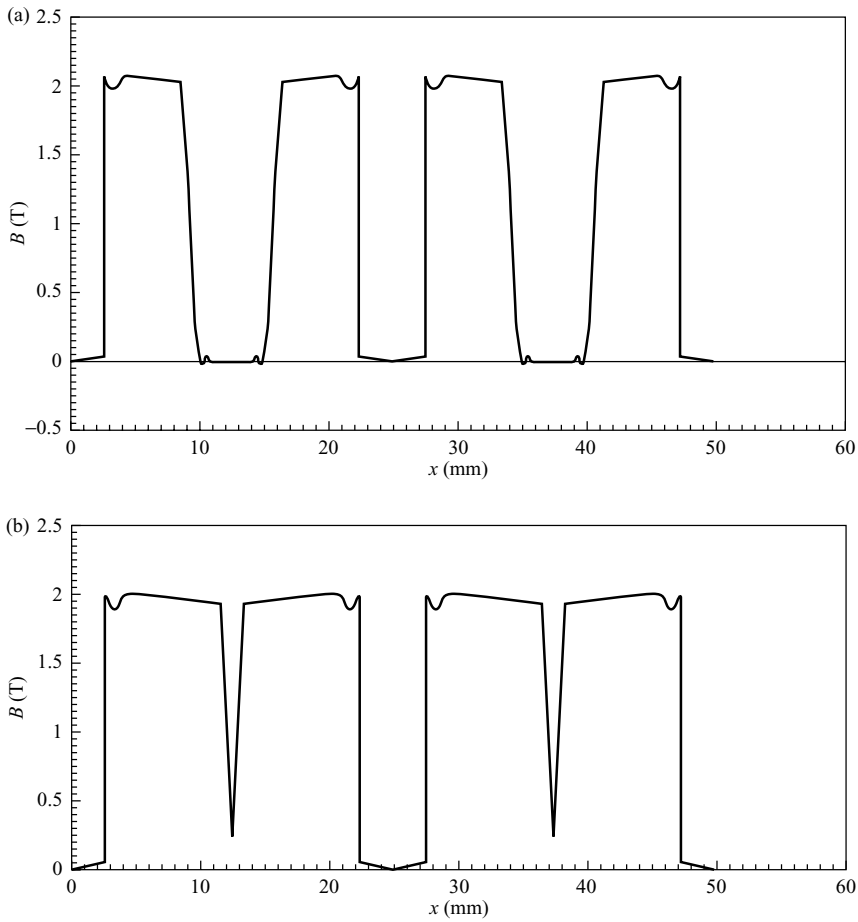

FIGURE E9.2.3 Computed magnetic flux density B versus position x in Figure E9.2.2 for $I = 2$ A and step B–H curve at times: (a) $t = 3$ ms, (b) $t = 6$ ms.

software computed the time for the flux density in the center of both steel legs to reach approximately half of its final value as 56 ms. This agrees well with 54.6 ms obtained using the linear formula (9.15).

Next, nonlinear transient analyses were performed. Since the slope of the *B–H* curve is used at each time step in Newton's method of Chapter 4, the infinite slope assumed for the step *B–H* curve of (9.23) must be replaced by a large finite slope. Here B_m is assumed to be 2 T and the slope from $B = 0$ to 1.93 T is assumed to be 100,000 times that of air. Above 1.93 T, the slope is gradually decreased to that of air at 2.07 T and higher. This step *B–H* curve is graphed in Figure B1 with data points listed in Table B2.1 of Appendix B.

Table E9.2.1 lists the values of τ_m for a range of H_o. The theoretical values of (9.23) are compared with finite-element computed values with the approximate step *B–H* curve. Note that the computed times agree closely with those of (9.23).

Table E9.2.1 also lists the computed nonlinear infusion times with the specified real steel *B–H* curve [1]. The real steel has an initial permeability of 630 times that of air for $B \ll 1$ T, and has a typical saturation knee that approaches the slope of air for $B \gg 2$ T. As expected, the real *B–H* curve produces different nonlinear infusion times. This "real" *B–H* curve is graphed in Figure B2 and has data points listed in Table B2.2 of Appendix B.

Figure E9.2.3 plots *B* versus position *x* in Figure E9.2.2 at two time steps of the finite-element analysis for 2 A and the step *B–H* of Table E9.2.1. Note the inward diffusion (infusion) of the step *B* from all four steel surfaces, as expected [4]. Figure E9.2.4 plots magnetic flux versus time for the same case. Since inductance is flux times *N/I*, the effective inductance also varies with time in the same manner.

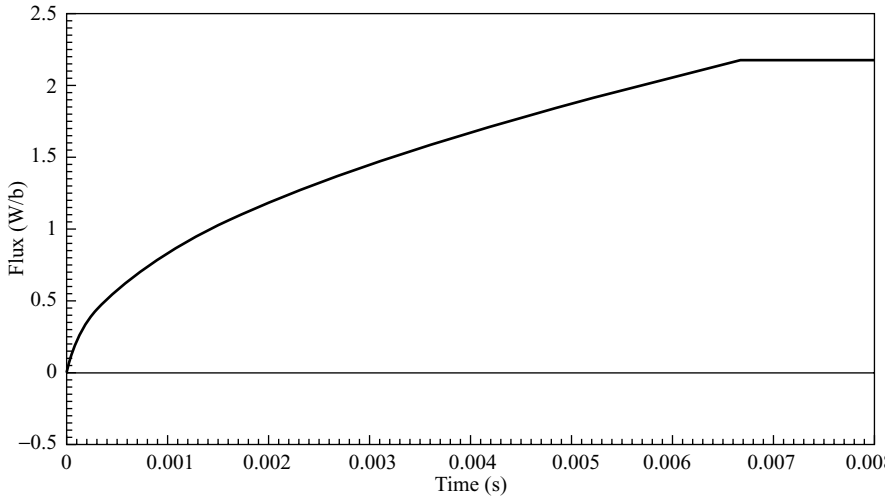

FIGURE E9.2.4 Computed magnetic flux versus time for $I = 2$ A and step *B–H* curve in Figure E9.2.2 with depth into page assumed to be 1 m.

9.4.3 Simple Equation for Steel Cylinder with "Step" *B–H*

To obtain an approximate formula for infusion time τ_m in nonlinear steel cylinders, first assume a "step" *B–H* curve as in the preceding section. Assuming the step curve for a steel cylinder of radius *R*, it has been found [4] that the magnetic field diffuses into the cylinder following a step wavefront at moving position $r_0(t)$. A formula [4] for the wavefront $r_0(t)$ derived for a field switched between $-B_m$ and $+B_m$ is here altered to account for a field switched from 0 to $+B_m$ by an applied $H_o(t)$:

$$2\int H_o dt/[\tfrac{1}{2}\sigma\ R^2\ B_m] = \lambda(\ln\lambda - 1) + 1 \tag{9.24}$$

where:

$$\lambda = r_0^2(t)/R^2 \tag{9.25}$$

The above two formulas are here applied to determine magnetic infusion time. Because the current is a step applied at time zero, H_o is also a step, and thus the left hand side of (9.24) has its integral over time replaced by $H_o\tau_m$. The value of λ is zero, since $r_0(t) = 0$ when $t = \tau_m$. Thus (9.24) becomes:

$$4H_o\,\tau_m/[\sigma\ R^2\ B_m] = 1 \tag{9.26}$$

giving [5]:

$$\tau_m = [\sigma\ R^2\ B_m]/[4H_o] \tag{9.27}$$

9.4.4 Transient Finite-Element Computations for Steel Cylinders

Transient finite-element analysis of the type used in Examples 9.1 and 9.2 can be used to compute diffusion into nonlinear steel cylinders. Various *B–H* curves may be input, both the preceding "step" curve of (9.27) and curves of actual steels.

Further studies of transient behavior of magnetic actuators will be presented in Chapters 14–16. They will show that mechanical motion can greatly affect the current waveform, magnetic flux, and magnetic force.

Example 9.3 Magnetic Infusion in Nonlinear Bessho Plunger Actuator An example of applying (9.27) is to the Bessho axisymmetric plunger actuator of Figure 5.2. Rather than modeling the entire actuator, a thin (10 mm) slice as shown in Figure E9.3.1 is to be modeled with 2D finite elements. The slice represents the armature (here assumed stationary with zero airgap), the coil, and the yoke. The purpose of the slice is to model only the variation of *B* with radial position *r*.

FIGURE E9.3.1 Slice (height 10 mm) of Bessho magnetic actuator, showing computed magnetic flux lines at $t = 20$ ms with actual B–H and $I = 0.5$ A.

Then

(a) The nonlinear infusion time is to be found using (9.27) assuming a step curve at $B_m = 2$ T for coil currents of 0.5 and 2 A. Also, find its magnetostatic flux lines using Maxwell and constant steel relative permeability of 630.

(b) Using Maxwell 2D or other available nonlinear transient finite-element software, confirm the results of (9.27) and then use the actual armature steel B–H curve given in [1] for 0.5 and 2 A coil currents.

Solution

(a) The infusion time τ_m for Figure E9.3.1 is found using (9.27) as follows. The radius $R = 0.020$ m from Figure 5.2. The applied field intensity H_o is found using Ampere's law for Figure 5.2:

$$H_o = NI/l \tag{E9.3.1}$$

where $N = 3300$. The path length l is assumed to be the 250-mm axial length of the coil window, meaning that the cylindrical core of radius 20-mm drops all ampere-turns (the outer yoke is assumed to have negligible MMF drop). The assumed B_m in steel is 2 T. Thus $I = 0.5$ A gives $H_o = 6600$ A/m. Substituting in (9.27) with the steel $\sigma = 1.7$E6 S/m gives $\tau_m = 51.5$ ms, which is listed in Table E9.3.1. The other analytical value listed in Table E9.3.1 is for the current quadrupled to 2 A, for which (9.27) obtains one-fourth the diffusion time, $\tau_m = 12.9$ ms. Note that both values are much less than the 93 ms obtained by the linear formula (9.20), and that the higher the current, the smaller the diffusion time.

TABLE E9.3.1 Bessho Actuator Nonlinear Magnetic Infusion Times (ms)

Current (A)	Analytical (9.21)	Finite Element (Step B–H)	Finite Element (Real B–H)
0.5	51.5	53.0	42.0
2.0	12.9	13.4	11.5

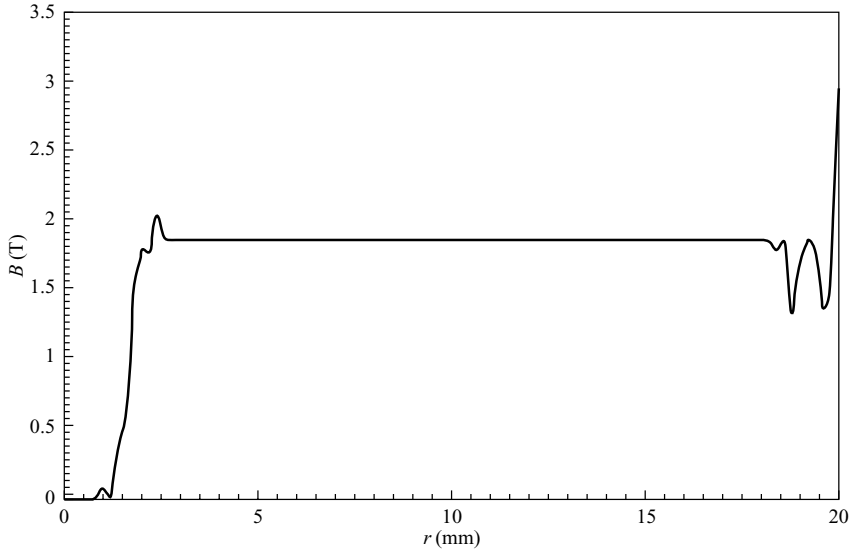

FIGURE E9.3.2 Flux density B (T) versus radius (mm) in core computed by nonlinear transient finite elements with step B–H curve at $t = 51$ ms.

(b) For the step B–H curve, finite-element analyses of Figure E9.3.1 were made with input currents of 0.5 and 2 A. Figure E9.3.2 shows the computed magnetic flux density waveshape in the core at a typical instant; note that it is a steep step to 2 T as expected. The time when the wavefront reaches zero radius is the magnetic diffusion time entered in Table E9.3.1. The computed diffusion (infusion) times agree well with the times predicted using (9.27).

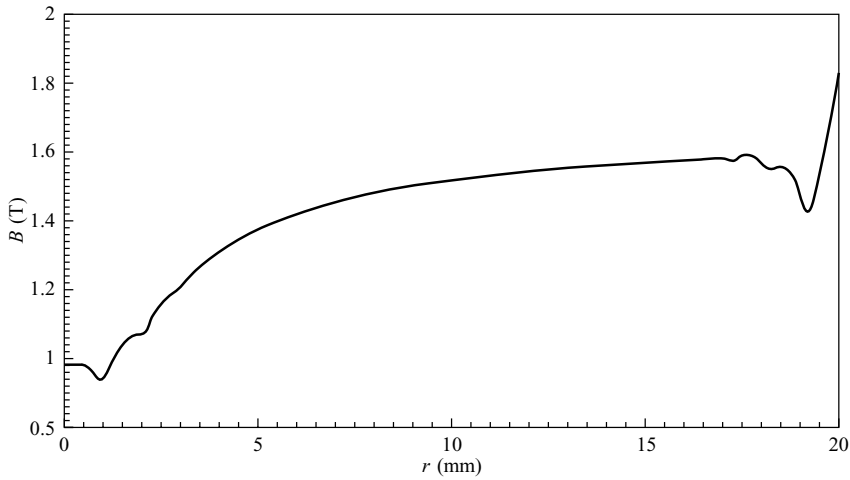

FIGURE E9.3.3 Flux density B (T) versus radius (mm) in core computed by nonlinear transient finite elements with actual B–H curve at $t = 40$ ms.

Other transient finite-element computations were then made using the actual Bessho core and yoke *B–H* curves. Figure E9.3.3 shows the computed flux density waveshape at a typical instant; note that it now has a more gradual rise. The computed infusion times with the actual *B–H* curves are also listed in Table E9.3.1. Note that *B–H* curve shape has a significant effect on the computed nonlinear infusion time.

9.5 NONLINEAR MAGNETIC EFFUSION TIME

This section examines effusion times, which apply when current and *H* have existed for at least several infusion times and are then suddenly turned off. The magnetic field *B* leaves or effuses from the conducting material with different effusion times for slabs and for cylinders. The nonlinear effusion times will in some cases be much longer than the nonlinear infusion times [6].

9.5.1 Planar Effusion in Nonlinear Steel Slab

Example 9.4 Magnetic Effusion in Nonlinear Rectangular Inductor The first example of nonlinear effusion is the rectangular inductor made of a conducting core that was shown in Figure E9.2.1. Its current is assumed to have flowed for a long time before it is turned off at time zero. The slice model of Figure E9.2.2 is to be used for initial currents of 0.1, 0.5, and 2 A with several different *B–H* curves to compute the flux decay.

Solution The finite-element model of Figure E9.1.2 is analyzed as follows [6] using Maxwell software. First, the "step" *B–H* curve of Figure B1 is input and the resulting flux density effusion (decay) is computed. The computed effusion flux density graphs versus position at a typical time after turnoff are shown in Figure E9.4.1. For the specified currents as well as a smaller one, Table E9.4.2 lists *B* values computed at typical times, where $B_{\max}$ is the maximum flux density (located in the center of each slab) at the given time.

Table E9.4.1 and Figure E9.4.1 show that for current *I* high enough to produce saturating flux density (above 2 T) with an assumed step *B–H* curve, the flux decay is very slow. The associated effusion time is thus very large, much larger than the 55 ms for constant permeability.

Because real steel *B–H* curves are not of step shape, the finite-element computations were repeated for the real *B–H* curve of Figure B2 with relative permeability 630 for *B* below 0.55 T. The initial currents being turned off are again $I = 0.1$, 0.5, and 2 A and the computed flux density graphs versus position at a typical time after turnoff are shown in Figure E9.4.2. For the same currents as well as a smaller one, Table E9.4.2 lists *B* values computed at typical times, where $B_{\max}$ is the maximum flux density (located in the center of each slab) at the given time.

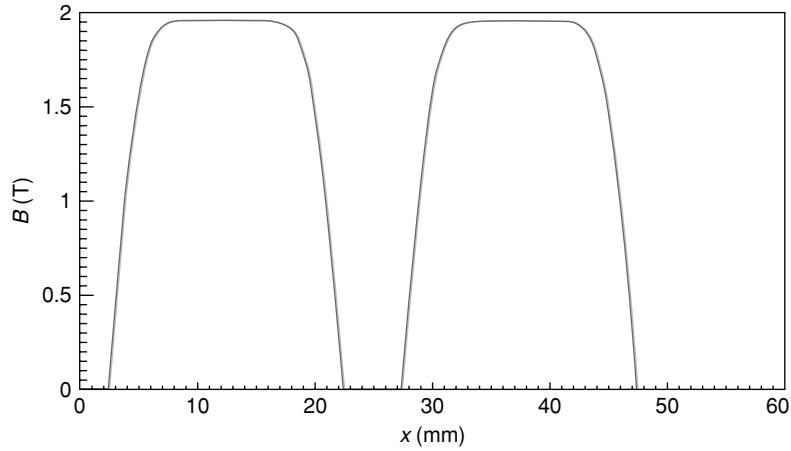

FIGURE E9.4.1 Computed effusion flux density distributions for "step" *B–H* curve in Figure E9.2.2 at time 50 ms after currents of 0.1, 0.5, and 2 A are turned off. The three distributions lie on top of one another.

TABLE E9.4.1 Effusion Flux Densities (T) Computed Versus Time for Planar Turnoff of Figures E9.2.2 and E9.4.1 with Nonlinear Step *B–H* Curve of Table B2.1

$I(t = 0)$ in A	$B(t = 0)$ in T	$B_{\max}(t = 0.05)$ in T
0.001	0.166597	0.16596
0.1	2.0349	1.9598
0.5	2.0655	1.9599
2.0	2.0926	1.960

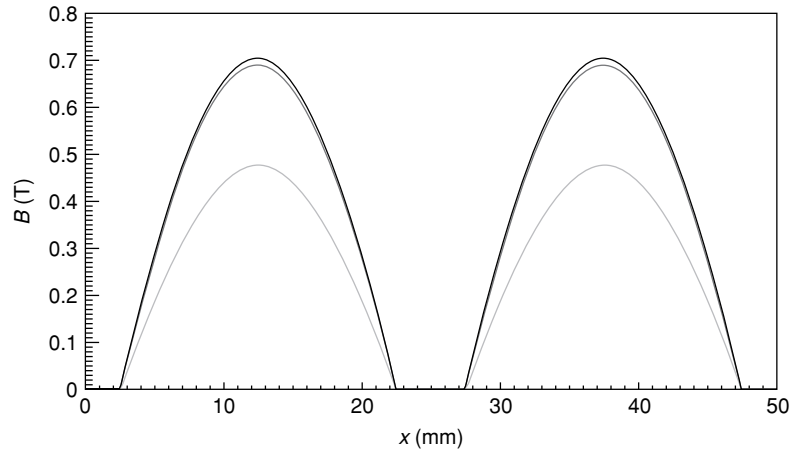

FIGURE E9.4.2 Computed effusion flux density distributions for real *B–H* curve in Figure E9.2.2 at time 50 ms after currents of 0.1, 0.5, and 2 A are turned off. The lowest curve is for the lowest current and the highest curve is for the highest current.

TABLE E9.4.2 Effusion Flux Densities (T) Computed Versus Time for Planar Turnoff of Figures E9.2.2 and E9.4.2 with Real Nonlinear *B–H* Curve of Table B2.2

$I(t = 0)$ in A	$B(t = 0)$ in T	$B_{max}(t = 0.05)$ in T	$B_{max}(t = 0.05)/B(0)$
0.01	0.10437	0.0532	0.510
0.1	0.97481	0.4775	0.490
0.5	1.6496	0.6909	0.419
2.0	1.8563	0.70568	0.380

TABLE E9.4.3 Magnetic Effusion Times (ms) Computed Using Finite-Element Analysis of Figures E9.2.2 and E9.4.2

$I(t = 0)$ in A	H_o in A/m	$\mu_r = 630$	Real *B–H*
0.01	132	55	55
0.1	1320	55	55
0.5	6600	55	47
2.0	26,400	55	42

Table E9.4.2 and Figure E9.4.2 show that the flux density is now decaying more rapidly with the real *B–H* curve. The associated effusion times are listed in Table E9.4.3.

Table E9.4.3 shows that the unsaturated results (for low current) agree with constant permeability results, as expected. Constant permeability results agree with the theory, showing equal infusion and effusion times. Table E9.4.3 also shows that with the real *B–H* curve, saturation produces only a gradual and small decrease in effusion time. The change in effusion time is much smaller than the huge reductions found in infusion time caused by saturation in Example 9.2. The results in Table E9.4.1 show that the step *B–H* curve is not appropriate for effusion modeling.

The reason why the step *B–H* curve is not appropriate for effusion models is evidently its extremely high permeability at low *H*. As permeability approaches infinity, linear diffusion time also approaches infinity, leading to nonlinear effusion times approaching infinity. Since real *B–H* curves at low *H* usually approach a constant (linear) permeability, real effusion times vary only slightly with saturation. In contrast, for infusion (turnon) the step *B–H* curve has the *B/H* ratio (called "secant permeability" or "apparent permeability") that decreases as *H* increases, and thus the step *B–H* curve is appropriate for turnon, and infusion times are similar for both step and real *B–H* curves.

Because a step *B–H* curve is too gross an approximation to obtain accurate effusion times, the next *B–H* curve investigated is a ramp *B–H* curve. The curve is shown in Figure B3 with points listed in Table B2.3 of Appendix B. It has an initial ramp with slope of a relative permeability of 630 that agrees with the initial permeability of the real *B–H* curve of Table B2.2. Near 2 T, the ramp is transitioned to the same slope μ_o of the step curve of Figure B1 with $B_m = 2$ T. Using this ramp *B–H* curve in the slice

TABLE E9.4.4 Effusion Flux Densities (T) Computed Versus Time for Planar Turnoff of Figure E9.2.2 with Ramp *B–H* Curve of Table B2.3

$I(t=0)$ in A	$B(t=0)$ in T	$B_{max}(t=0.05)$ in T	$B_{max}(t=0.05)/B(0)$
0.01	0.1045	0.0534	0.512
0.1	1.0452	0.5336	0.511
0.5	2.0528	1.0050	0.490
2.0	2.0871	1.0080	0.483

model of Figure E9.2.2 for several currents, the computed results are summarized in Table E9.4.4.

Comparing Table E9.4.4 with Table E9.4.2, it is seen that turnoff with the ramp *B–H* curve agrees only somewhat with the real curve. Comparing Tables E9.4.4, E9.4.2, and E9.4.1, the ramp *B–H* curve does yield somewhat more accurate turnoff results than the step *B–H* curve. For truly accurate effusion prediction, however, the real *B–H* curve must be used. Thus the simple formula (9.23) for step *B–H* curves is only applicable for infusion time, and is not applicable for effusion time. In addition, if any formulas were to be derived for nonlinear saturable effusion time, they would have to contain multiple variables to account for actual *B–H* curve shape, not just the single variable B_m of step *B–H* curves.

9.5.2 Axisymmetric Effusion in Nonlinear Steel Cylinder

Example 9.5 Magnetic Effusion in Nonlinear Bessho Plunger An axisymmetric example of nonlinear effusion is due to turnoff of current flowing in the cylindrical plunger slice model shown in Figure E9.3.1. The current is assumed to have flowed for a long time before it is turned off at time zero. The model of Figure E9.3.1 includes the cylindrical plunger of the Bessho actuator, and is to be analyzed using Maxwell finite-element software first for constant permeability and then for initial currents of 0.1, 0.5, and 2 A. Since the preceding Example 9.4 showed that step and ramp *B–H* curves do not give accurate effusion times, here only the real *B–H* curve will be used in Maxwell finite-element software.

Solution The axisymmetric finite-element model pictured in Figure E9.3.1 is first analyzed with constant relative permeability equal to 630 and with 10 A current turned off at $t = 0$. At $t = 0$, the computed flux density throughout the cylindrical plunger is 0.7557 T. At $t = 93$ ms, the computed flux lines are shown in Figure E9.5.1 and the flux density versus radius is graphed in Figure E9.5.2. It shows that surface flux density is approximately zero, but the flux density at zero radius is 0.43391 T. The ratio of (0.43391/0.7557) = 57.4%, reasonably close to the 58.8% of (9.21).

For the real nonlinear *B–H* curve of Figure B2 and Table B2.2 of Appendix B, the computed *B* versus radius at $t = 90$ ms is graphed in Figure E9.5.3 for the three

FIGURE E9.5.1 Slice model (height 10 mm) of Bessho actuator with computed flux lines 93 ms after current turnoff with constant steel relative permeability of 630.

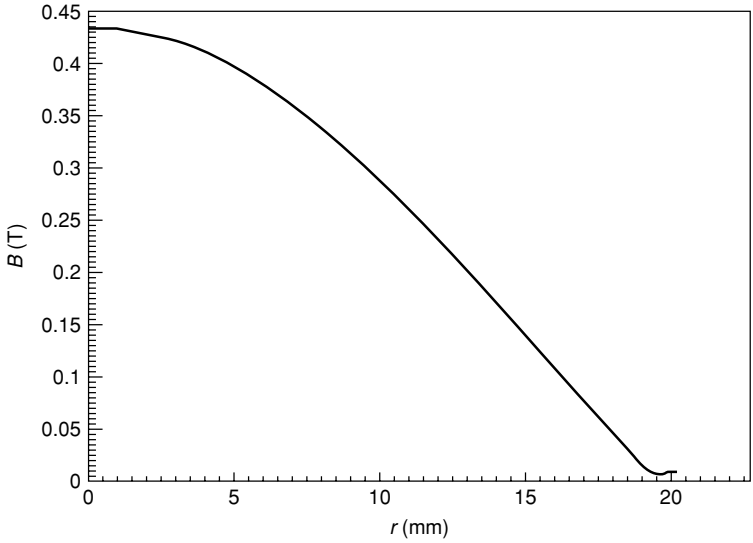

FIGURE E9.5.2 Computed effusion flux density versus radius 93 ms after current turnoff in Bessho cylindrical slice model with constant relative permeability of 630, as in Figure E9.5.1.

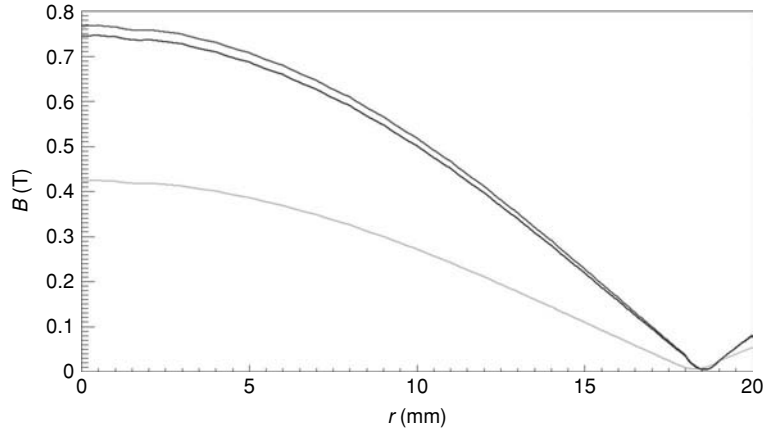

FIGURE E9.5.3 Computed effusion flux density distributions for real *B*–*H* curve in Bessho actuator at $t = 90$ ms after currents of 0.1, 0.5, and 2 A are turned off. The lowest curve is for the lowest current and the highest curve is for the highest current.

TABLE E9.5.1 Effusion Flux Densities (T) Computed Versus Time for Axisymmetric Cylinder Turnoff of Figure E9.5.1 with Real *B–H* Curve

$I(t=0)$ in A	$B(t=0)$ in T	$B_{\max}(t=0.09)$ in T	$B_{\max}(t=0.09)/B(0)$
0.01	0.0997	0.06742	0.676
0.1	0.7829	0.4250	0.543
0.5	1.6209	0.7476	0.461
2.0	1.8453	0.7698	0.417

TABLE E9.5.2 Magnetic Effusion Times (ms) Computed Using Finite-Element Model of Cylinder of Figure E9.5.1

$I(t=0)$ in A	H_o in A/m	$\mu_r = 630$	Real *B–H*
0.01	132	93	93
0.1	1320	93	84
0.5	6600	93	70
2.0	26,400	93	58

input currents. For the same currents as well as a smaller one, Table E9.5.1 lists B values computed at typical times, where $B_{\max}$ is the maximum flux density (located at zero radius) at the given time. For currents above 0.01 A, the slice model assumes the actual yoke *B–H* curve, whereas at the lowest current the yoke is assumed to have relative permeability of 10,000 as in Figures E9.5.1 and E9.5.2. Because the cross-sectional area of the yoke is proportional to the difference between the squares of its outer and inner radii, its area is 36% larger than the cylindrical plunger, and thus its MMF drop is much less than that of the plunger. Also, because the yoke has radial thickness of only 4 mm, much smaller than the 20-mm plunger radius, its flux diffuses much faster than the plunger flux. Thus the yoke has only a minor effect on MMF drops and the results, and it is not included in the calculated applied H values in Tables E9.5.1 and E9.5.2.

Table E9.5.2 lists the computed effusion times for the various input currents. It shows that the unsaturated results (for low current) agree with constant permeability results, as expected. Constant permeability results agree with theory, showing effusion time of 93 ms, the same as the linear infusion time. Table E9.5.2 also shows that saturation produces only a gradual and rather small decrease in effusion time. The reduction in effusion time caused by saturation is much smaller than the huge reductions in saturated infusion time.

9.6 PULSE RESPONSE OF NONLINEAR STEEL

In many cases, currents and surface **H** fields are pulsed [7–9]. The excitation is turned on and then off. Thus the magnetic flux densities and the flux in conducting steel

are expected to first rise with an infusion time and then to fall with an effusion time. Since the infusion and effusion times in nonlinear steel may differ considerably, the flux rise and fall times may differ if the steel has flux densities in its nonlinear region.

Example 9.6 Flux Rise and Fall in Conducting Slabs The coil current in the planar steel slabs of Figure E9.2.2 is zero before $t = 0$, when it is switched to 2 A. At $t = 30$ ms the current is switched back to zero. Find the flux linkage of the coil versus time for $0 < t < 80$ ms using the actual steel B–H curve.

Solution The Maxwell 2D planar transient finite-element solution produced the flux linkage graph in Figure E9.6.1. The expected infusion time is 5 ms from Table E9.2.1, while the expected effusion time is 42 ms from Table E9.4.3. These two times correspond respectively with the rise and fall times observable in Figure E9.6.1. Due to saturation, the fall time is over eight times the rise time.

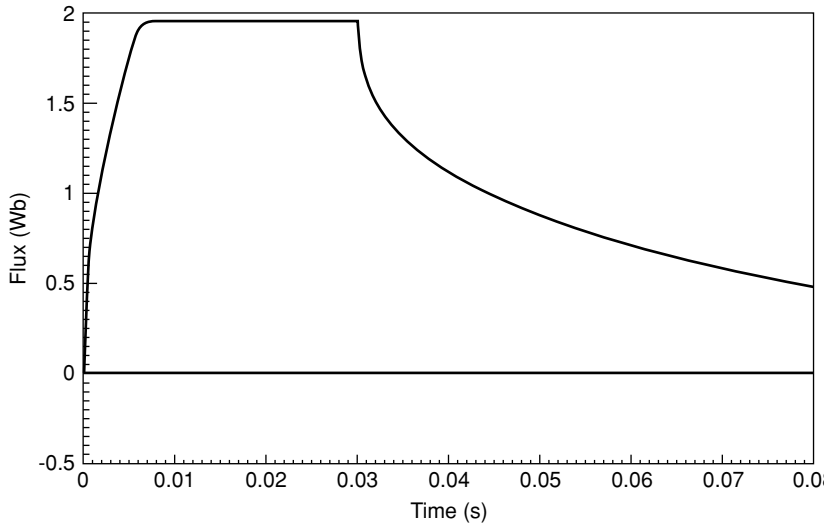

FIGURE E9.6.1 Computed flux linkage versus time for the slabs of Figure E9.2.2 with the real B–H curve and $I = 2$ A turned on at $t = 0$ and turned off at $t = 30$ ms.

Example 9.7 Flux Rise and Fall in a Conducting Cylinder The coil current in the axisymmetric slice model of the Bessho actuator in Figure E9.3.1 is zero before $t = 0$, when it is switched to 2 A. At $t = 30$ ms the current is switched back to zero. Find the flux linkage of the coil versus time for $0 < t < 90$ ms using the actual (real) steel B–H curve.

Solution The Maxwell 2D axisymmetric transient finite-element solution produced the flux linkage graph in Figure E9.7.1. The expected infusion time is 11.5 ms from

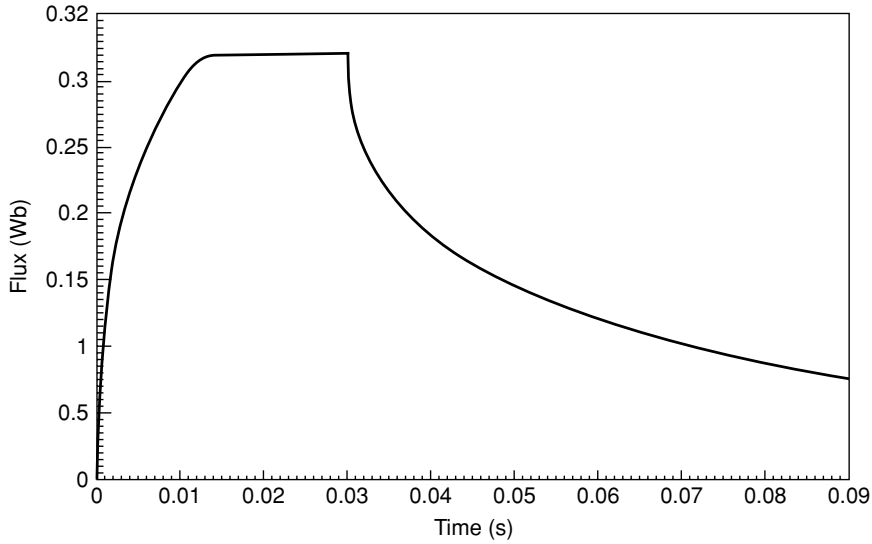

FIGURE E9.7.1 Computed flux linkage versus time for the cylindrical slice model of Figure E9.5.1 with the real *B–H* curve and $I = 2$A turned on at $t = 0$ and turned off at $t = 30$ ms.

Table E9.3.1, while the expected effusion time is 58 ms from Table E9.5.2. These two times correspond respectively with the rise and fall times observable in Figure E9.7.1. The fall time is over five times the rise time due to saturation.

PROBLEMS

9.1 Find the maximum acceleration and minimum operation time for a smaller version of the Bessho actuator, in which all dimensions are reduced by 50%.

9.2 Find the analytic diffusion time for the steel with the properties of Example 9.1a but with its width reduced by a factor of (a) 10, (b) 100, and (c) 1000.

9.3 Redo Example 9.1b and 9.1c using Maxwell but with its width reduced by a factor of 10.

9.4 Redo Example 9.1b and 9.1c using Maxwell but with its width reduced by a factor of 100.

9.5 Redo Example 9.1b and 9.1c using Maxwell but with its width reduced by a factor of 1000.

9.6 Put a 1-mm airgap at the upper armature/stator interface of Problem 9.3 and repeat the computations of Problem 9.3. Show that the airgap produces significant changes in the flux pattern.

9.7 Figure P9.7.1 shows a sector of a toroidal inductor with a circular (cylindrical) core. It extends into the page to a depth of 1 m. The core is made of solid steel and has inner radius $r_i = 10$ mm and outer radius $r_o = 30$ mm. Only a 4° sector of the 360° of the circular inductor is shown and to be modeled; this smaller model saves computer time. Inside the inner radius is a coil carrying ampere-turns NI in the $+z$ (out) direction, where $NI = 4.608$ or 9.215 ampere-turns. Outside the 30-mm core radius, to a radius of 31.6 mm, the coil ampere-turns are returned as $-NI$. The eddy currents in the core must sum to zero.

(a) Apply the nonlinear infusion time formula to find infusion times for both given ampere-turns. Note that because two different H_o values exist due to its differing inner and outer path lengths, you will only find a range of infusion times for each value of ampere-turns.

(b) Use Maxwell 2D to obtain infusion times by nonlinear transient finite-element analyses with the real B–H curve of the Bessho armature steel.

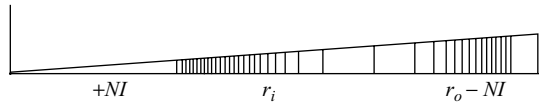

FIGURE P9.7.1 Four-degree sector of circular inductor with inner core radius $r_i = 10$ mm and outer core radius $r_o = 30$ mm. The flux lines at 10 ms are computed with windings of $NI = 4.608$ A and with the real B–H curve. Note that the flux lines are diffusing inward from both steel core surfaces.

9.8 Figure P9.8.1 shows a laminated core inductor mounted in a solid-steel cabinet. The cabinet is made of solid-steel panels on all of its six sides. Inductors are often placed inside such cabinets to house them mechanically and to confine their magnetic fields and thereby reduce electromagnetic interference. The cabinet (also called a box or a housing) is known to often increase the inductance. However, the inductance increase is delayed by the magnetic diffusion time of the solid-steel panels.

The inductor of Figure P9.8.1 has N_T total turns placed in the center of a steel cabinet. Because the inductor core is laminated or made of composite ferromagnetic material with extremely low electrical conductivity, the electrical conductivity of the core is assumed to be zero. Thus eddy currents exist only in the solid-steel panels. Figure P9.8.2 is a 2-mm high slice of the right half of Figure P9.8.1. It includes only the right half of the center leg, the right coil half and the right panel, which has an eddy current that does not sum to zero. The eddy current in the right panel is returned through the other five cabinet panels.

Because the coil is only on the inside of the steel panel and its eddy currents can be returned through the other five cabinet panels, diffusion only occurs into the inside of the panel. Thus w must be considered to be twice the panel thickness T, giving:

$$\tau_m = \sigma\,(2T)^2\,B_m/(8H_o) = \sigma\,T^2\,B_m/(2H_o) \qquad \text{(P9.8.1)}$$

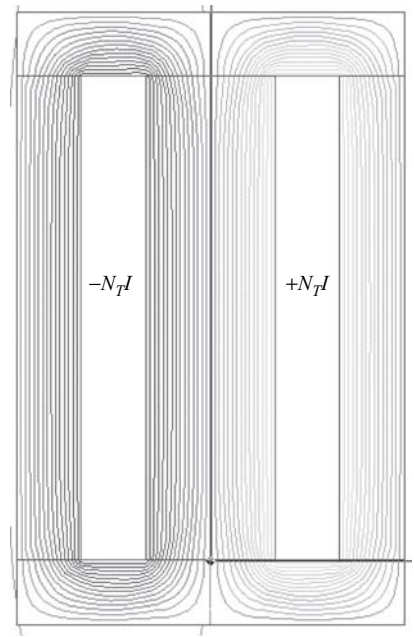

FIGURE P9.8.1 Computer display of laminated inductor core surrounded by solid-steel panels on all four sides, showing typical magnetostatic (no eddy current) flux lines computed by Maxwell. The overall dimensions are 95 mm high and 60 mm wide. The four panels are all 10 mm thick. The laminated center core is 20 mm thick.

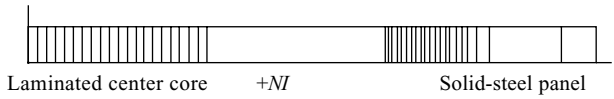

FIGURE P9.8.2 Two millimeter high section of right half of inductor of Figure P9.8.1 with computed flux lines at time $t = 6$ ms and $I = 0.5$ A for real B–H curve. Note that the flux lines are diffusing into the panel from the coil ampere-turns NI, but that the flux lines in the laminated core are uniform due to its lack of eddy currents.

The core material is here assumed to be laminated SAE 1010 steel with the B–H curve given in Maxwell. The outer shell is assumed to be made of solid steel with conductivity 1.7E6 S/m. The number of conductors N in Figure P9.8.2 is assumed to be 26.4.

(a) Find the analytic infusion times for a step B–H curve at 2 T and currents of 0.5, 1, and 2 A.

(b) Verify the results of (a) using Maxwell 2D or other software, and then repeat using the actual Bessho armature B–H curve [1].

REFERENCES

1. Bessho K, Yamada S, Kanamura Y. Analysis of transient characteristics of plunger type electromagnets. *Electr Eng Japan* 1978;98:56–62.
2. Brauer JR. Magnetic actuator models including prediction of nonlinear eddy current effects and coupling to hydraulics and mechanics. *Proc Congresso Brasileiro de Eletromagnetismo*, Gramado, Brazil, November 2002.
3. Woodson HH, Melcher JR. *Electromechanical Dynamics*, Part II. New York: John Wiley & Sons; 1968.
4. Mayergoyz ID. *Nonlinear Diffusion of Electromagnetic Fields*. San Diego, CA: Academic Press; 1998.
5. Brauer JR, Mayergoyz ID. Finite element computation of nonlinear magnetic diffusion and its effects when coupled to electrical, mechanical, and hydraulic systems. *IEEE Trans Magn* 2004;40:537–540.
6. Brauer JR. Magnetic diffusion times for infusion and effusion in nonlinear steel slabs and cylinders. *IEEE Trans Magn* 2007;43:3181–3188.
7. Bendre A, Divan D, Kranz W, Brumsickle W. Are voltage sags destroying equipment? *IEEE Industry Appl Mag* 2006;12:12–21.
8. Bíró O, Preis K. An efficient time domain method for nonlinear periodic eddy current problems. *IEEE Trans Magn* 2006;42:695–698.
9. Ausserhofer S, Bíró O, Preis K. An efficient harmonic balance method for nonlinear eddy current problems. *IEEE Trans Magn* 2007;43:1229–1232.